Characterising Metal-Insulator Transitions in the Aubry-André Model Using the de Broglie-Bohm Interpretation

Student Number: 1522275

Department of Physics, University of Warwick, Coventry CV4 7AL, United Kingdom

The Aubry-André model is shown to exhibit a metal-insulator transition by applying the alternative de Broglie-Bohm interpretation of quantum mechanics. A computer simulation is used to examine the Bohm trajectories of a particle guided by a gaussian pilot wave in one dimension. The particle is shown to change from a free to a localised state with increasing Aubry-André potential strength. An addition to the simulation is proposed for future work which would make the necessary calculations less computationally intensive and improve the accuracy and precision of the results.

I. Introduction

A metal-insulator transition (MIT) is identified as a rapid change from a conductive metallic phase, where the electron wave functions are extended throughout the system, to an insulating phase where wave functions are localised. Understanding the mechanisms of MITs remains a focus of fundamental research [1, 2]. Continuing to develop our understanding of how the change in electrical resistance of many orders of magnitude may be controlled offers a wealth of potential applications, from resistive switching random access memory [3] to energy saving thermochromic films [4]. This project investigates the particular case of the MIT in the Aubry-André (AA) model using the alternative de Broglie-Bohm (dBB) interpretation of quantum mechanics. To the author's knowledge dBB theory has never previously been applied to localisation problems. Using this alternative approach has the potential to reveal features of the MIT and the AA model which are not immediately apparent using the traditional Copenhagen interpretation [5]. Agreement of these results with those found using the Copenhagen interpretation could have implications for fundamental quantum theory, which is of pro-

found importance in all of modern physics.

II. Theory

A. The Aubry-André Model

According to the scaling hypothesis of localisation, an MIT occurring due to disorder will not generally exist in systems with less than three spatial dimensions [6]. The AA model [7] however, is a quasi-periodic model which exhibits an MIT that occurs as a function of varying quasiperiodic potential strength, even in one dimension [8]. The existance of an MIT in one dimension, along with the relative simplicity of the model make it a useful tool for examining the physics of an MIT at the single particle level. An experimental realisation of the AA model is the use of a Bose-Einstein condensate to create a one-dimensional lattice perturbed by a second, weak incommensurate lattice [10].

The AA model is a special case of the one-dimensional tight binding model [11]. In the tight binding model, the valence electrons are imagined to have wave functions equal to those of isolated atoms. As shown in fig. 1, where the atoms exist in a one dimensional lattice chain and their separation is decreased, the atomic orbitals will begin to overlap and it is possible for an electron to transfer between atoms. This can be described for the change of an electron on the nth atom in the chain to a neighboring atom as a change from state ϕ_n to state ϕ_{n+1} or ϕ_{n-1}.

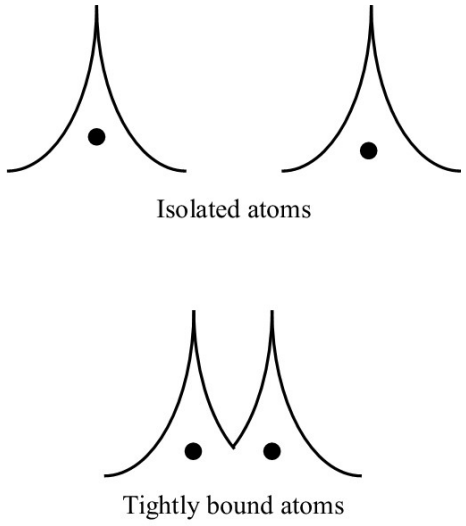

Figure 1: Wave functions of two atoms in the one dimensional tight binding model.

Therefore the schrödinger equation of a single particle in the AA model is [8]

$$\phi_{n+1} = (E - \mu_n)\phi_n - \phi_{n-1}, \qquad (1)$$

where ϕ_n is the wavefunction of the particle on atom n, E its energy and μ_n is the onsite potential.

In contrast to the ordinary tight binding model, the AA model represents a quasi-periodic lattice [12] where the potential is given by

$$\mu_n \equiv 2\mu\, cos(\alpha n + \beta) \qquad (2)$$

with potential strength μ, $\alpha/2\pi$ an irrational number and β an arbitrary phase shift. In this project $\alpha/2\pi$ was selected as the inverse of the golden mean such that

$\alpha/2\pi = (\sqrt{5}-1)/2$. It can be shown that the golden mean is approximated by the ratio of sucessive Fibonacci numbers.

Previous work [7, 8] suggests that the MIT in the AA model exists at $\mu = 1$. An important feature of the AA model is that in the case of a single particle [13], its properties follow from the Harper equation [9], for which the spectrum is a cantor set with a dense set of gaps [14]. As a result all states in the model are either extended, critical or localised and the MIT should have no energy dependence. Therefore it is expected that this study should also show the MIT to occur at $\mu = 1$

B. de-Broglie Bohm Theory

The de Broglie-Bohm (DBB) or pilot wave theory used in this study to investigate the MIT in the AA model, is an alternative interpretation of quantum mechanics, which can be shown to produce the same results as the Copenhagen interpretation. The theory states that a system is comprised of a point particle guided on a 'Bohm trajectory' by a wave described by the wavefunction $\Psi(x,t)$ that satisfies the Schrödinger equation [16]. This motivation for this interpretation can be summarised as follows [15]:

Consider the polar form of the one dimensional wavefunction

$$\Psi(\mathbf{x},t) = Re^{\frac{iS}{\hbar}} \tag{3}$$

where $R = R(\mathbf{x},t)$ and $S = S(\mathbf{x},t)$. By substituting (3) into the Schrödinger equation

$$i\hbar\frac{\partial}{\partial t}\Psi(\mathbf{x},t) = \Big[-\frac{\hbar^2}{2m}\nabla^2 + V(\mathbf{x},t)\Big]\Psi(\mathbf{x},t) \tag{4}$$

and seperating real and imaginary parts ((5) and (6) respectively) we obtain

$$\frac{\partial S}{\partial t} + \frac{(\nabla S)^2}{2m} - \frac{\hbar^2}{2m}\frac{\nabla^2 R}{R} + V(\mathbf{x},t) = 0 \tag{5}$$

$$\frac{\partial R^2}{\partial t} + \nabla\cdot\Big(\frac{R^2\nabla S}{m}\Big) = 0 \tag{6}$$

where the functions R(**x**,t) and S(**x**,t) codetermine each other.

(5) is of the same form as the classical Hamilton-Jacobi equation (where S is Hamilton's principle function)

$$\frac{\partial S}{\partial t} + \frac{(\nabla S)^2}{2m} + V(\mathbf{x},t) = 0 \tag{7}$$

with an extra potential term

$$\frac{-\hbar^2}{2m}\frac{\nabla^2 R}{R} = Q(\mathbf{x},t) \tag{8}$$

the 'quantum potential'. Expressing (5) in this notation reveals it to be a generalised form of the Hamilton-Jacobi equation:

$$\frac{\partial S}{\partial t} + \frac{(\nabla S)^2}{2m} + V(\mathbf{x},t) + Q(\mathbf{x},t) = 0 \tag{9}$$

It can be shown that from the solution to (9), the equation of motion of the particle

guided by Ψ is

$$\dot{\mathbf{x}} = \frac{\nabla S(\mathbf{x}, t)}{m}\Big|_{\mathbf{x}=\mathbf{x}(t)}. \tag{10}$$

To solve (10) for $\mathbf{x}$ and find the trajectory of the particle for all time, an initial position $\mathbf{x_0}$ is required. The DBB interpretation proposes that rather than a quantum system being inherently probabilistic as described by the Copenhagen interpretation, the probabilistic nature of quantum mechanics arises from a practical, but not fundamental inability to measure or control the initial conditions of the particle with sufficient precision between successive measurements. By solving (10) for varying initial conditions, an ensemble of possible particle trajectories is found. DBB theory postulates that to be consistent with the Born rule, the probability that a particular initial position in the ensemble lies between $\mathbf{x}$ and $\mathbf{x}+\mathrm{d}\mathbf{x}$ is $R^2(\mathbf{x}, t_o)$ where $R^2 = |\Psi|^2$. It is worth noting recent work [17], which suggests that over long time periods the ensemble of trajectories evolves to eventually satisfy the Born rule, even where the initial conditions do not. Therefore it is possible that the Born rule arises as a natural consequence of the underlying physics of the dBB interpretation, rather than being a necessary assumption.

III. Methodology

A. Simulation

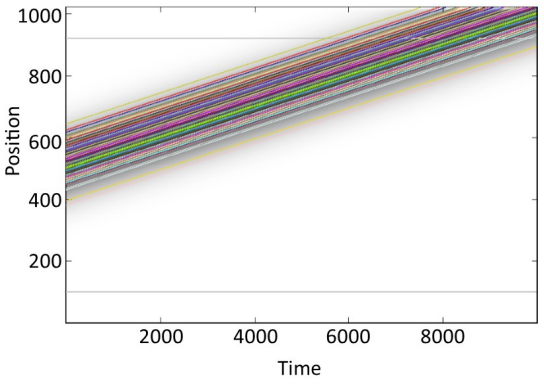

Figure 2: A typical output of the simulation where Bohm trajectories are shown in colour and $|\Psi|^2$ shown in black

A computer simulation was used to calculate the Bohm trajectories of a particle guided by a gaussian wave packet in one dimension. The inverse golden mean in (2) is approximated by the simulation as the ratio of successive Fibonacci numbers for the purpose of calculating the potential. From a specified initial wave function, ensemble of initial positions, energy and AA potential (2), the simulation calculates the wave function each time step by Chebyshev propagation [18]. This requires the use of a dispersion relation of the form

$$E = \frac{1 - cos(k)}{m} \tag{11}$$

where E and k are the energy and wavenumber of the wavepacket respectively. The gradient of the phase $\nabla S(x, t)$ is integrated to calculate the position of the

trajectories at each time step. A typical output from the simulation is shown in fig.2

An ensemble of 100 trajectories was used with their initial positions 'Born distributed'; placed at random in a region of fixed width, where the probability of being placed at a given position x was proportional to the value of the initial wavefunction squared $|\Psi(x,0)|^2$ at that position.

B. Characterising the MIT

The average velocity $\bar{\bar{V}}$ of the ensemble of trajectories was plotted as a function of potential strength μ for a range of energies and system sizes. $\bar{\bar{V}}$ was calculated as

$$\bar{\bar{V}} = \sum_{i=0}^{n} \frac{\widetilde{V}_i P_i}{n} = \sum_{i=0}^{n} \frac{\widetilde{V}_i |\Psi_0(x)|^2}{n}. \qquad (12)$$

$\widetilde{V}_i$ is the velocity of a particular trajectory, n is the number of trajectories and P_i is the probability that the particle has an initial position x such that it follows trajectory i, which is equal to the modulus squared of the initial wavefunction, $|\Psi_0(x)|^2$. As the initial positions were Born distributed, the probability term in (1) was already encoded into the initial positions and the average velocity was calculated as

$$\bar{\bar{V}} = \sum_{i=0}^{n} \frac{\widetilde{V}_i}{n}. \qquad (13)$$

Each $\widetilde{V}_i$ was evaluated as illustrated in fig.3. Tangent approximations were made to each trajectory every ten time steps, between t = 100 time steps and 100 time steps before the first trajectory hit a boundary. This avoided the influence of any boundary effects. The gradient v_{ij}, (where ij denotes the jth tangent on the ith trajectory), of each of the tangent approximations was found and their mean calculated to find $\widetilde{V}_i$ for a given trajectory as

$$\widetilde{V}_i = \sum_{j=0}^{m} \frac{v_{ij}}{m}, \qquad (14)$$

where m is the number of tangent approximations made per trajectory.

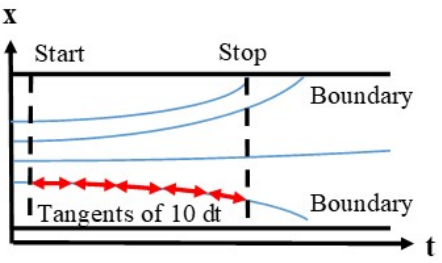

Figure 3: The tangent approximation which was calculated every ten time steps to find the velocities $\widetilde{V}_i$ of Bohm trajectories in an ensemble. Not to scale.

The error in $\bar{\bar{V}}$ was estimated by considering each value of $\widetilde{V}_i$ to be a result of independent repeated measurements of the velocity of the wavepacket which were combined to give a best estimate of $\bar{\bar{V}}$. Because the simulation randomly generates the initial positions according to the Born distribution, the results are equivalent to those of a real experiment where the velocity of the wavepacket is repeatedly measured and each result is random and independent with

an associated error. In this case the error arises predominantly from the use of tangent approximations to trajectories which are often curved. Therefore as described in [19], the error in $\widetilde{V}_i$ was estimated as the standard deviation of the tangent approximations to a trajectory, and the error in $\bar{\bar{V}}$ was found from (2) using the functional approach.

To characterise the transitions, linear fits were made as shown in fig.4 over two points above and below the half way point between the maximum and minimum velocity. Two points were chosen as a range which was well approximated by a linear fit, based on the mean residual sum of squares as described in results. The critical value μ_c was defined as the x intercept of a fit to serve as a measure of the strength of the transition.

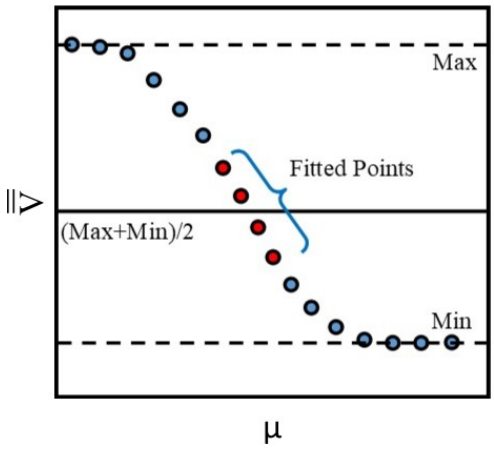

Figure 4: The fitting of data to find μ_c

IV. Results

Fig. 5 shows the plots of $\bar{\bar{V}}$ against μ for varying energy and system size. The error bars appear to be overestimated, which relates to the random number generation in the Born distribution of initial positions and is explained further in the discussions. The least squares linear fits are also shown, which were made over two points either side of half of the maximum velocity as described in methodology. Due to the large error bars using χ^2_v to assess the suitability of the fit was not possible. Instead a fitting range of four points was chosen on the basis that the mean residual sum of squares increased exponentially for greater numbers of points, and was less than 10^{-4} for all energies using four points, making it a good linear approximation.

Fig. 6 shows μ_c plotted as a function of system size for each energy. Also plotted is μ_{cAve}, calculated as the error weighted mean of μ_c for corresponding positive and negative energy to reduce systematic error. The error in average μ_c was estimated as the standard deviation of the two μ_c found from positive and negative energy. Fig. 7 shows μ_c and μ_{cAve} for different system sizes as a function of energy.

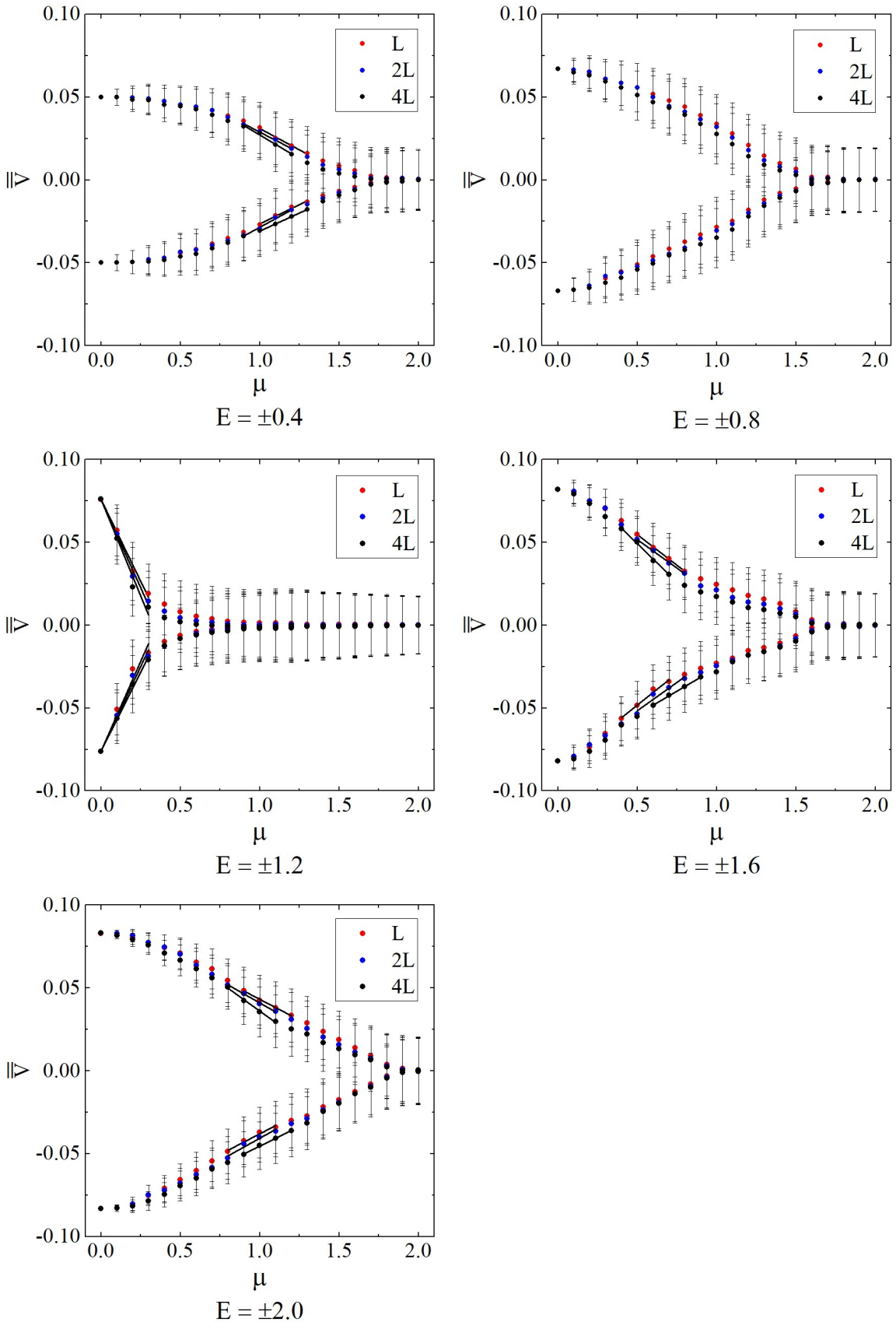

Figure 5: MIT in the AA model as found using de Broglie-Bohm theory for various energies and system sizes with least squares linear fits to find μ_c for each.

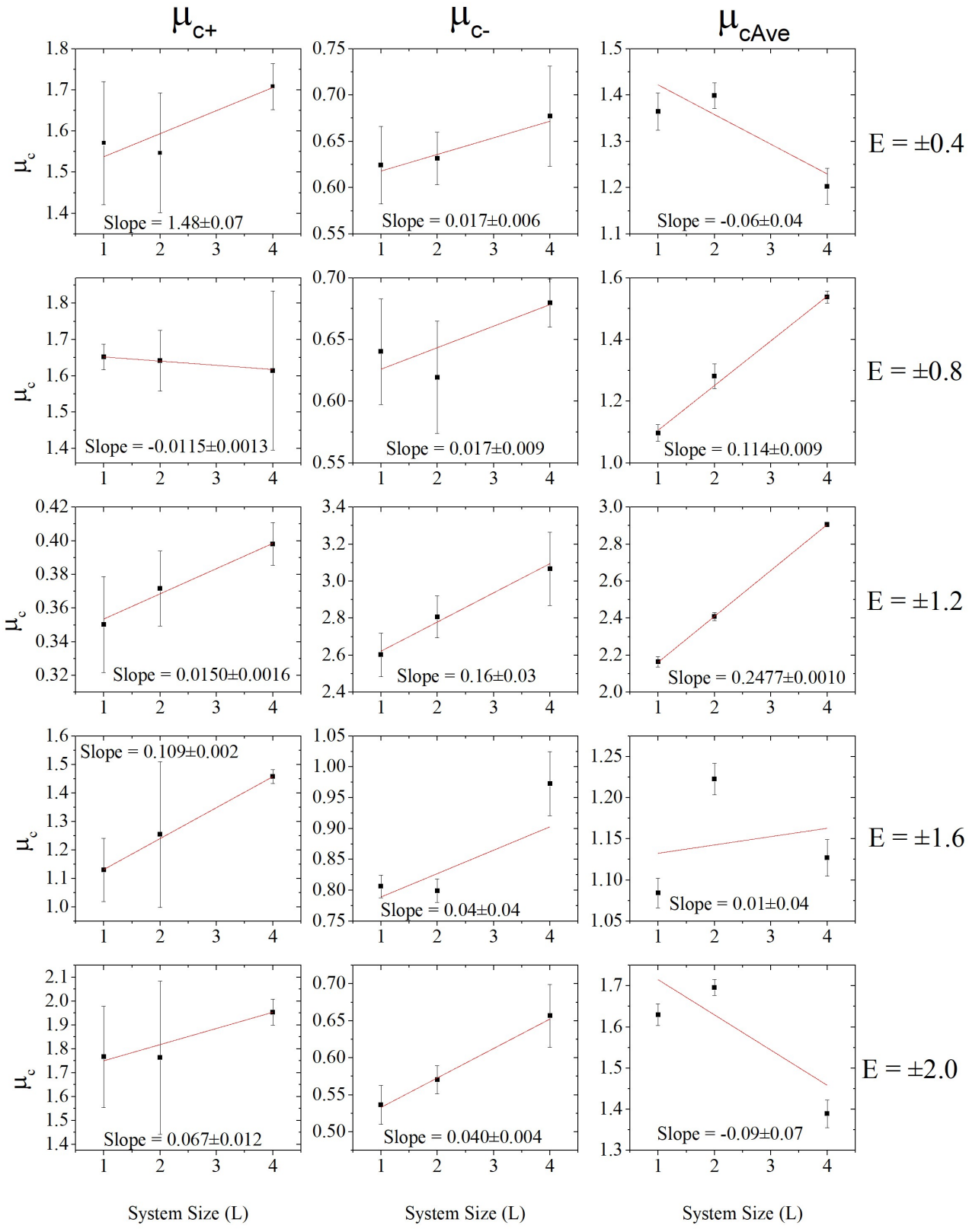

Figure 6: The effect of varying system size on AA MIT strength

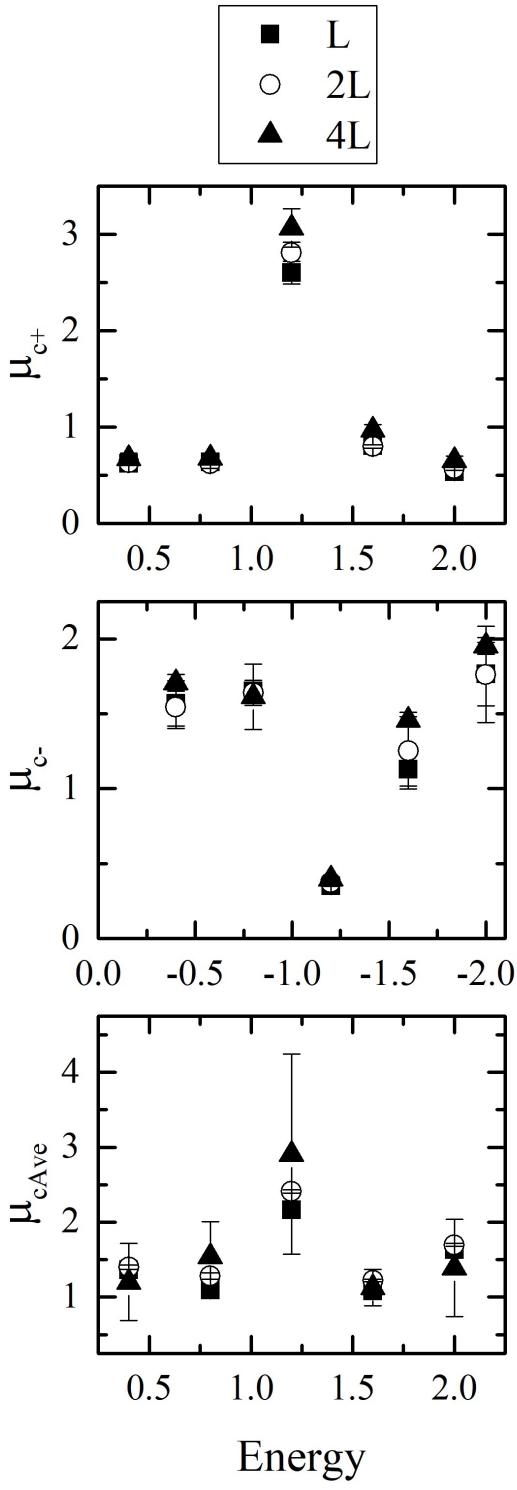

Figure 7: The effect of varying energy on AA MIT strength

V. Discussions

From fig. 5, it can be seen that as μ increases, $\bar{\bar{V}}$ decreases to zero velocity. Therefore the Aubry-André model can be shown to exhibit an MIT using a de Broglie-Bohm approach. Fig. 5 does not appear to show the MIT to be at $\mu = 1$ as expected. Nor is the location of the MIT the same for different energies.

It is possible that these unexpected results are related to the cause of the apparently over-estimated error bars. In the Born distribution of the initial positions, the simulation calculates the random placement from a user defined seed. In a real experiment, the ensemble of initial positions would be necessarily different for every measurement. In the simulation this would correspond to using a different seed for every value of μ for which a velocity was found. Because of the way the simulation generates data files it was not possible to vary the seed for each measurement without exceeding the storage space available on the computer systems used. Therefore the same seed was used giving rise to the same initial positions for every value of velocity found introducing false correlation into the data.

Fig.8 shows $\bar{\bar{V}}$ for ten different seeds with energy $= 0.4$ and $\mu = 1$. The seeds were produced by a true random number generator seeded by the user's keyboard input. It can be seen that the resulting spread in $\bar{\bar{V}}$ is approximately 0.01. While this is of the correct magnitude to match the error bars in fig. 5, it is not a large enough spread to

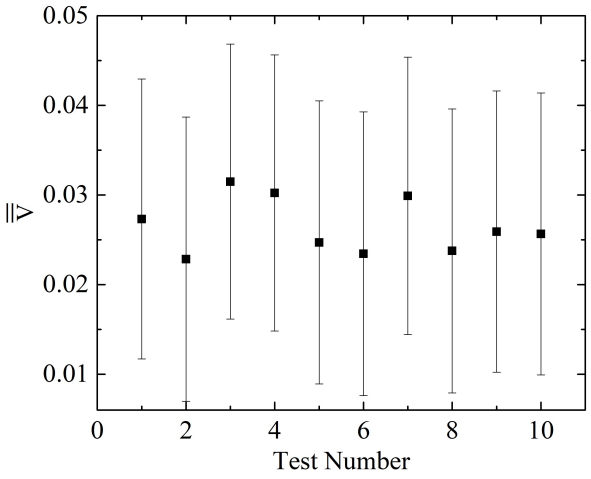

Figure 8: Randomly varying the seed changes $\bar{\bar{V}}$

completely account for the variation in the position of the MIT. Further points would need to be tested to assess how the true spread varies with energy and μ. If more time and resources were available, a truly random seed should be used for every point as well as a larger number of trajectories. In the appendix, an alternative means of distributing the initial positions in proportion to the wave function is proposed which would both improve the precision of the results for a given number of trajectories and eliminate the need for a random seed.

It would be expected that all aspects of the plots in fig. 5 should be symmetrical for corresponding positive and negative energies. While there is general symmetry, a systematic offset can be seen between different system sizes, where larger system sizes are most negatively offset for values of μ around 1. It is thought that this relates to the dispersion of the wavepacket, in combination with the constant seed. The standard deviation of V_i was plotted as a function of μ to see how the dispersion varied with potential strength (not shown here). No obvious relation could be found other than that dispersion is virtually zero at $= 2$ $\mu = 0$ and $\mu = 2$ with some increase at other μ. As shown in fig. 9, the lowest trajectories curve until they reach some constant negative velocity. These trajectories reduce

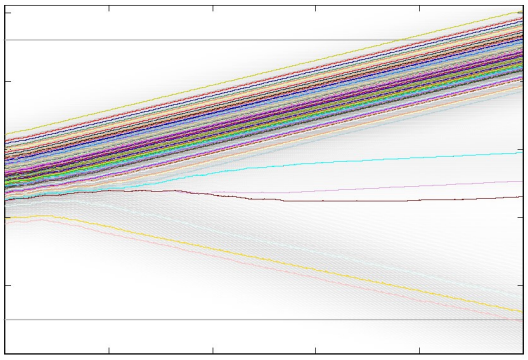

Figure 9: Dispersion of the wavepacket

the value of $\bar{\bar{V}}$. In larger system sizes the outer trajectories will have constant negative velocity for a longer time period, and therefore contribute more to reducing $\bar{\bar{V}}$. The use of the constant seed is likely to have introduced some constant asymmetry into the trajectories. This would make them more likely to disperse in a particular direction on average irrespective of the sign of the energy, introducing a systematic offset. Further study of the dispersion for other seeds, system sizes and μ may reveal interesting behaviors. Further study of the dispersion for other seeds, system sizes and μ may reveal interesting behaviors

Most plots in fig. 6 suggest a positive linear relation between μ_c and system size. Generally the strength of a transition increases with increasing system size [20], which would mean μ_c should decrease with increasing system size. The slope of the fit varies greatly between plots for different energies as well as corresponding positive and negative energies. By eliminating the systematic errors in fig. 5 as discussed it may be possible to establish some clearer relation. Finding μ_c for a greater number of system sizes would make it possible to determine if the relation is indeed linear. It was not possible to do this due to the simulation requiring system size to be changed by a factor of two, which meant insufficient storage space was available for a complete set of data at larger system sizes.

The variance of μ_c with energy is further highlighted in fig. 7. For positive and negative energies alone no clear relation is apparent. For μ_{cAve} however, at least four of the five values are the same within the error bar for each system size. This suggests that it may be possible to eliminate the variation with energy by the means previously discussed with further time and resources.

VI. Conclusions

This research shows that it is possible to demonstrate an MIT in the AA model using de Broglie-Bohm theory. To the authors knowledge, this is the first study to do so. This result provides evidence that the alternative interpretation can serve as a useful tool for investigating quantum systems.

Relatively few quantitative conclusions can be drawn from the current data due to the problem of being unable to change the seed with the time and computing resources available. Nonetheless, the methods of analysing the MIT developed during this study lay the foundations for future work. With the implementation of the proposed method of distributing initial positions of the trajectories, it would be possible to further characterise the MIT found. In particular, the exact location of the MIT, its lack of energy dependence and the effect of larger system sizes could all be determined.

Appendix - Function Distributed Trajectories

While the Born distribution of initial positions currently implemented in the simulation is representative of a real world experiment, it poses various challenges as discussed due to the large amounts of data which must be generated to produce accurate results using this method. Here an alternative method of distributing the initial positions in proportion to a general initial $|\psi|^2$ is proposed. The new method would

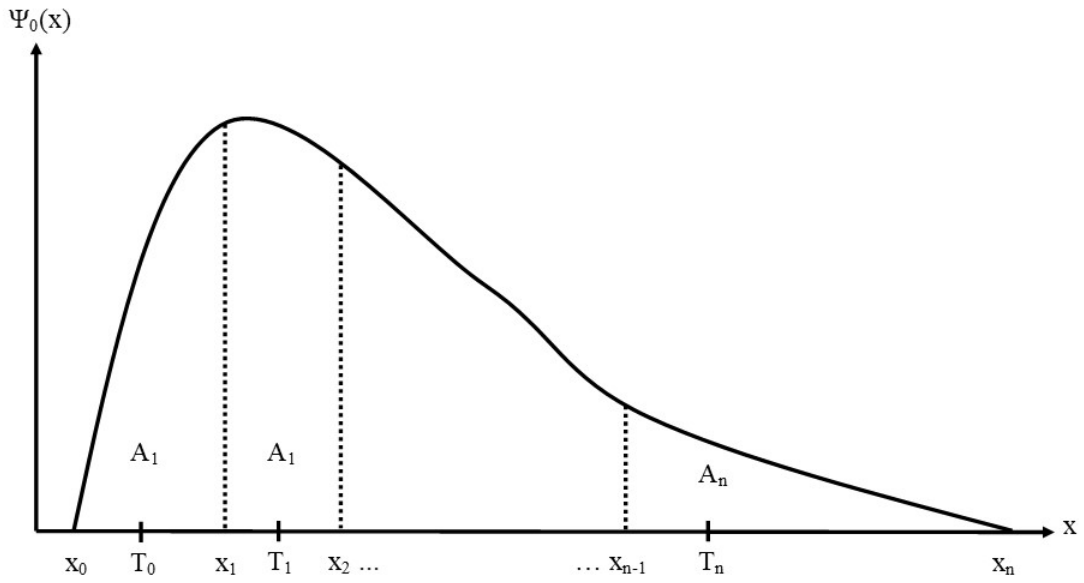

Figure 10: 'Function Distribution' of trajectories

produce accurate results using fewer trajectories without requiring random number generation, and therefore be less computationally intensive and require less storage.

To encode the probability term of (10) into the initial positions, the space between trajectories should be proportional to $|\psi|^2$. Therefore as shown in fig.10, let the initial position of each trajectory T_i in an ensemble of n trajectories be located on the centroid in x of regions of equal area A_i bounded by $\Psi_0(x)$ and the x axis between some positions $x_i - x_{i-1}$.

Where $\Psi_0(x)$ is normalised,

$$\sum_{i=0}^{n} A_i = 1. \tag{15}$$

Therefore

$$A_i = \frac{1}{n} = \int_{x_{i-1}}^{x_i} \Psi_0(x)dx. \tag{16}$$

A centroid between specified bounds is calculated as

$$\bar{x} = \frac{\int x\Psi_0(x)dx}{\int dx} \tag{17}$$

Therefore the positions T_i can be calculated as

$$T_i = \frac{\int_{x_{i-1}}^{x_i} x\Psi_0(x)dx}{\int_{x_{i-1}}^{x_i} dx} \tag{18}$$

By integrating numerically solve (16) for each x_i, (18) can be evaluated to find each T_i.

This method is given the name 'function distribution'. It effectively approximates an initial distribution of an infinite number of trajectories Born distributed for any given wave function. The accuracy of the approximation improves with increasing n.

References

[1] M. L. Ndawana, R. A. Rmer, M. Schreiber Europhys. Lett. **68**, 678 (2004)

[2] Edoardo G. Carnio, Nicholas D. M. Hine, R. A. Rmer submitted to Phys. Rev. Lett., (2017)

[3] S. Kim, Y. Chang, M. Kim, T. Kim, Y. Kim, B. Park , 10 **5**, 459 Materials (2017)

[4] D. Zhang, H. Sun, M. Wang, L. Miao, H. Liu, Y. Zhang, J. Bian Materials **10**, 314 (2017).

[5] https://plato.stanford.edu/entries/qm-copenhagen/ (Accessed March 2018)

[6] E. Abrahams, P.W. Anderson, D.C. Licciardello, T.V. Ramakrishnan, Phys. Rev. Lett. **42**, 673 (1979).

[7] S. Aubry, G. Andre, Ann. Israel Phys. Soc. **3**, 133 (1980).

[8] A. Eilmes, U. Grimm, R.A. Römer, M. Schreiber Eur. Phys. J. B **8**, 547 (1999).

[9] P.G. Harper, Proc. Phys. Soc. London A **68**, 874 (1955).

[10] G.Roati *et al.*, Nature **453**, 895 (2008).

[11] T. Mishra, R. Shashidhara, T. G. Sarkar, J. N. Bandyopadhyay Phys. Rev. A **94**, 053612 (2016)

[12] F. Duan J. Guojun *Introduction to Condensed Matter Physics Volume 1* (World Scientific 2005) 2.3

[13] V.Mastropietro Phys. Rev. Lett. **115**, 180401 (2015).

[14] A. Avila and S. Jitomirskaya, Ann. Math. **170**, 303 (2009).

[15] P.R. Holland *The Quantum Theory of Motion: An Account of the de Broglie-Bohm Causal Intperpretation of Quantum Mechanics* (Cambridge University Press, 1993).

[16] D.Bohm, Phys.Rev **85**, 166 (1952).

[17] M. D. Towler, N. J. Russel, A. Valentini Proc. R. Soc. A **468**, 9901013 (2012)

[18] H. Guo Chebyshev Propagation and Applications to Scattering Problems (2004) In: A. Lagana, G. Lendvay (eds) Theory of Chemical Reaction Dynamics. NATO Science Series II: Mathematics, Physics and Chemistry (II. Mathematics, Physics and Chemistry), vol 145. Springer, Dordrecht

[19] I.G. Hughes, T.P. Hase *Measurements and their Uncertainties* (Oxford University Press, 2013) 4.5.

[20] V. Khemani, S.P. Lim, D.N. Sheng, and D.A. Huse Phys. Rev. X **7**, 021013 (2017)